Faculty of Women for, Arts, Science, and Education

Scientific Publishing Unit

Journal of Scientific Research in Science

Basic Sciences

Volume 41, Issue 1, 2024

ISSN 2356-8372 (Online) \ ISSN 2356-8364 (print)

Journal of Scientific Research in Science 2024, 41, (1),141:158

Contents lists available at EKB

Journal of Scientific Research in Science

Journal homepage: https://jsrs.journals.ekb.eg/

Assembly of a nanostructured $NiCo_2S_4/NiS_2/Co_9S_8$ composite for enhanced electrochemical performance in symmetric supercapacitors.

Reham Ehab Mostafa[1,*], S. S. Mahmoud[1], N. S. Tantawy[1], and Saad G. Mohamed[1].

[1]Chemistry Department, Faculty of Women for Arts, Science and Education, Ain Shams University, Cairo, Egypt.
[2]Mining and Metallurgy Engineering Department, Tabbin Institute for Metallurgical Studies (TIMS), Tabbin, Helwan 109, Cairo 11421, Egypt.

Abstract

Bimetallic transition metal sulfides (TMSs) exhibit considerable potential for energy storage. However, to keep improving the performance of electrochemical systems, effective synthetic techniques for advantageous electrode architecture still need to be developed. The present study involved the synthesis of a $NiCo_2S_4/NiS_2/Co_9S_8$ nanocomposite (NCS/NS/CS) employing polyethyleneimine by the solvothermal technique, resulting in the creation of an NiCo-precursor. After that, we annealed the NiCo-precursor with S powder for two hours at 300 °C in an argon atmosphere. The enhanced morphology and NCS/NS/CS electrode conductivity allow for fast ion transport, giving them an excellent electrochemical energy storage feature. At 0.5 A/g, the NCS/NS/CS nanocomposite displays a capacitance of 326 F/g. Additionally, utilizing an NCS/NS/CS electrode for each of the positive and negative electrodes, an NCS/NS/CS//NCS/NS/CS symmetric device was created, providing an exceptional 18.9 Wh k/g of specific energy at a specific power of 529 W k/g at 1 A/g. According to these, the NCS/NS/CS nanocomposite is an excellent choice for an electrode material with remarkable performance in supercapacitors.

Keywords: NCS/NS/CS composites; Symmetric supercapacitor; Solvothermal; Battery-type materials.

***corresponding author**: **, Reham Ehab Mostafa**, Chemistry Department, Faculty of Women for Arts, Science and Education, Ain Shams University, Cairo, Egypt.
Email: rehamehab@chem.gov.eg
(Received 22 Dec 2023, revised 1 Feb 2024, accepted 15 Feb 2024)
https://doi.org/10.21608/JSRS.2024.257240.1122

1. Introduction

Owing to fossil fuel overuse and their finite supply, which raises serious environmental issues, we are currently experiencing an energy crisis that is forcing us to look for ecologically friendly energy sources [1-3]. So, supercapacitors (SCs) have been characterized by their excellent power density, extended and steady life cycle, near-maintenance-free nature, easy charging and discharging circuit requirements, overall increased safety, and capacity for overcoming the energy/power deficit that exists between fuel cells/batteries and the capacitor [4, 5]. With respect to the phenomenon of energy storage, SCs could be categorised into three distinct classes: First, electric double-layer capacitors (EDLCs), whose capacitance results from the electrode/electrolyte contact's charge storage and mostly works with materials like activated carbon and graphene, Since EDLC is a surface storage system, the electrode materials' surface properties, such as surface area and permeability, determine how well this type of supercapacitor performs [6, 7]. and the second is pseudocapacitors, which concentrate on conducting polymers (CPs) and metal oxides like NiO [8], MnO_2 [9] and Co_3O_4 [10]. Their capacitance derives from the quick Faradaic redox processes that take place in the electrode material. The use of CPs as an effective electrode material is limited by their poor durability [6]. The third category is known as battery-type materials, which may store charges by typical Faradaic processes while also storing charges through the bulk of the electrode/electrolyte contact (non-capacitive) like metal sulfides and oxides [11-14].

Lately, transition metal sulfides (TMSs) have proved more appropriate as electrodes for SCs due to their larger capacitance, greater redox sites, and superior conductivity compared to transition metal oxides (TMOs) and hydroxides. These benefits may be attributed to the fact that sulfur has low electronegativity and is more flexible, which facilitates easier electron transit and increased electrochemical activity [15, 16]. The morphologies of $NiCo_2S_4$ have changed recently, affecting its capacity to store energy. These morphologies involve mesoporous [17], hierarchical [18], nanowires [19], nanorods [20], hollow spheres [21], nanotubes [22], and nanoflakes [23]. By using a solvothermal method, Zhang et al. were capable of manufacturing $NiCo_2S_4$ nanosheets that reveal an outstanding capacitance of 957 F/g at 1 A/g [24]. Xu et al. created a $NiCo_2S_4/Co_9S_8$ composite through a two-stage hydrothermal approach, resulting in an electrode with exceptional electrochemical properties [20]. Using a single-step hydrothermal procedure,

Wang et al. synthesized $NiCo_2S_4$@RGO, which has at 1 Ag^{-1} a superb capacitance of 2003 F/g [25]. Xionga et al. created $NiCo_2S_4$ nanostructured using an easy hydrothermal technique, displaying at 1 A/g a remarkable capacitance of 1154 F/g. The asymmetric device at 1 A/g demonstrates an energy of 17.3 Wh k/g [26]. Hierarchical $NiCo_2S_4$@CoS_2 was developed by Govindasamy et al. The nanostructure electrode, obtained using the hydrothermal technique, demonstrates a capacitance of 1565 F/g at 1 A/g. The device demonstrated a power output of 242.8 W k/g, corresponding to an energy of 17 Wh k/g [27].

$NiCo_2S_4$'s electronic conductivity may be enhanced by incorporating it with conductive materials, such as carbonaceous compounds, which act as a template. Thus, branched polyethyleneimine PEI is a polyamine derivative whose structure includes a significant amount of primary, secondary, and tertiary amines that are chemically active. This qualifies it as a good precursor for creating functional materials with more intriguing properties [28, 29].

In this study, the synthesis of a $NiCo_2S_4$/NiS_2/Co_9S_8 nanocomposite (NCS/NS/CS) employs polyethyleneimine by the solvothermal technique, resulting in the creation of an NiCo-precursor. After that, we annealed the NiCo-precursor with S powder for two hours at 300 °C in an argon atmosphere. The enhanced morphology and NCS/NS/CS electrode conductivity allow for fast ion transport, giving them an excellent electrochemical energy storage feature. At 0.5 A/g, the NCS/NS/CS nanocomposite displays a capacitance of 326 F/g. Additionally, utilizing an NCS/NS/CS electrode for each of the positive and negative electrodes, an NCS/NS/CS//NCS/NS/CS symmetric device was created, providing an exceptional 18.9 Wh k/g of specific energy at a specific power of 529 W k/g at 1 A/g.

2. Experimental section

2.1. Synthesis of NiCo-precursor (NC-precursor)

Solvothermal synthesis was used to create the NC-precursor. Dissolved were 0.5 mmol of $Co(NO_3)_2 \cdot 6H_2O$ and 0.5 mmol of $Ni(NO_3)_2 \cdot 6H_2O$, with 15 mmol of urea in 30 ml of a branched polyethyleneimine PEI solution in absolute ethanol (5:95% wt/vol.). PEI was utilized as the matrix for the NC-precursor since it is a rich supply of carbon and nitrogen and possesses chelating properties. The aforesaid solution was then gradually stirred for 1 hour while adding 5 mmol of NH_4F to create a brown solution, then put inside a 50-ml Teflon-lining autoclave and

heated at 140°C for 12 hours. NC-precursor solid precipitates were produced. The solid disc was then left to dry overnight at 60°C after being cleaned with deionized water and ethyl alcohol.

2.2. Synthesis of $NiCo_2S_4/NiS_2/Co_9S_8$ (NCS/NS/CS)

After grinding the NC precursor, use it in a mass ratio of 1:5 with sulfur powder. Subsequently, they were annealed at 300 °C for 2 hours in an argon atmosphere. The NCS/NS/CS were obtained. The schematic diagram in Fig. 1 depicts the general method of synthesis.

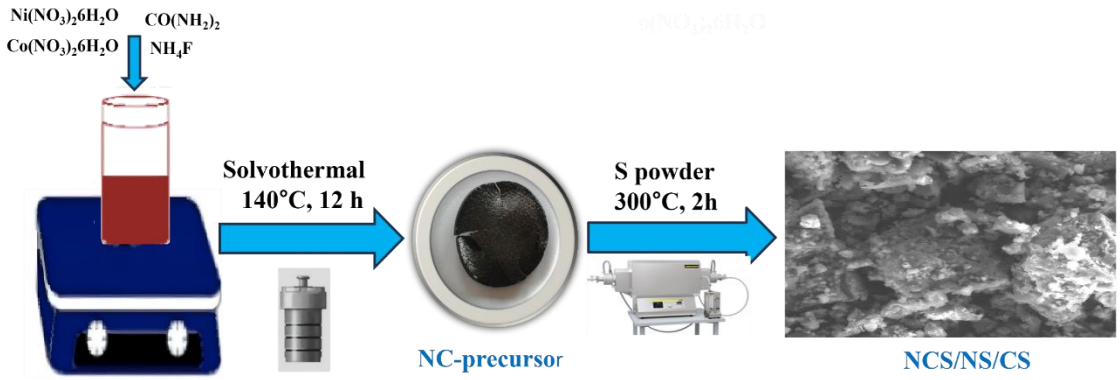

Fig. 1: A schematic illustration showing the NCS/NS/CS overall synthesis procedure.

2.3. Characterizations

Crystallographic characteristics and phase purity of the fabricated electrodes were measured using an X-ray diffractometer (Bruker AXSD8, ADVANCE, Germany). Surface morphologies and structures were investigated via a field emission scanning electron microscope (FESEM, Quattro S, Thermo Scientific).

2.4. Electrochemical Measurements

Three electrodes were used for the electrochemical tests: 6M KOH was employed as the electrolyte, and the counter and reference electrodes were provided by a platinum wire and a saturated calomel electrode (SCE). The created materials act as the working electrodes, which were made via the drop-casting technique with a completely blending slurry containing 8 mg of active materials, 1 mg of conductive carbon black, 20 µl of Nafion in a weight ratio of 80:10:10, and 750 µl of ethanol as solvent. After applying the prepared homogenous slurry to 1 cm x 3 cm of nickel foam NF, it was scrubbed with acetone and a 30% HCl solution while being sonicated

to guarantee that any oxide layers were removed. Overnight drying was given to the electrodes at 70 °C once they had been thoroughly coated.

The electrochemical measurements were performed by a (Voltalab 40 PGZ 301, Radiometer Analytical, France) electrochemical workstation consisting of cyclic voltammetry (CV) measurements performed at various scan rates within an operational potential. Galvanostatic charge-discharge (GCD) measurements took place at various current densities, employing the matching GCD discharge curve. Eqs. (1) and (2) [30, 31] were used to compute the specific capacitance C_S and specific capacity C. To evaluate the supercapacitive behaviour, electrochemical impedance spectroscopy (EIS) was applied.

$$\boldsymbol{Cs} = \frac{\boldsymbol{2I\int Vdt}}{\boldsymbol{mV^2}} \quad [Fg^{-1}] \quad (1)$$

$$\boldsymbol{C} = \frac{\boldsymbol{Idt}}{\boldsymbol{m}} \quad [Cg^{-1}] \quad (2)$$

where (V) stands for the applied potential window (V), (I) refers to the applicable current (A), (m) denotes the active electrode mass, (dt) indicates the time required for discharging (s), and (∫ Vdt) denotes the integral area of voltage against discharge time.

Similarly, given similar CV curves, the specific capacity Q may be determined by employing the working electrode's subsequent Eq. (3) [28, 30].

$$\boldsymbol{Q} = \frac{\boldsymbol{\int IdV}}{\boldsymbol{2mv}} \quad [Cg^{-1}] \quad (3)$$

For every CV curve, ∫IdV stands for the integral area of voltage versus current, and v ($V\ s^{-1}$) provides the potential scan rate.

For practical use, a symmetric device was established that employed NCS/NS/CS on NF as both a positive and negative electrode, a separator constructed of filter paper, and 6 M KOH as electrolyte (referred to as NCS/NS/CS//NCS/NS/CS). Just as with the three-electrode configuration, precise measurements were taken after assembly.

The device's specific energy (E_d) and matching specific power (P_d) were obtained by employing Eqs. 4 and 5 below [32-34].

$$E_d = \frac{I \int V dt}{3.6m} \quad [\text{Wh kg}^{-1}] \quad (4)$$

$$P_d = \frac{3600 E_d}{\Delta t} \quad [\text{W kg}^{-1}] \quad (5)$$

Where (m) (g) denotes the active material mass, ∫Vdt denotes the area under the appropriate discharge profile, and (Δt) indicates the discharge time (s).

3. RESULT AND DISCUSSIONS

3.1. Material Characterization

As seen in the XRD of various materials. An amorphous structure is observed in the NC-precursor, as Fig. 2 shows, and after being annealed into NCS/NS/CS, the peaks located at 2θ of 16.6°, 31.8°, 38.6°, 50.7°, 55.5°, 58.5°, 65.2°, 69.4°, and 78.3° can be attributed to the planes (111), (311), (400), (511), (440), (531), (533), (444), and (731) of the $NiCo_2S_4$ phase (JCPDS Card No.00-020-0782). In the NiS_2 (JCPDS Card No. 01-080-0377), the peaks at 27°, 35°, and 46.1° are related to the (111), (210), and (220) planes. In the Co_9S_8 phase (JCPDS Card No.01-086-2273), peaks occur at 25°, 47.6°, and 52.1°, which are attributed to the (220), (511), and (440) planes.

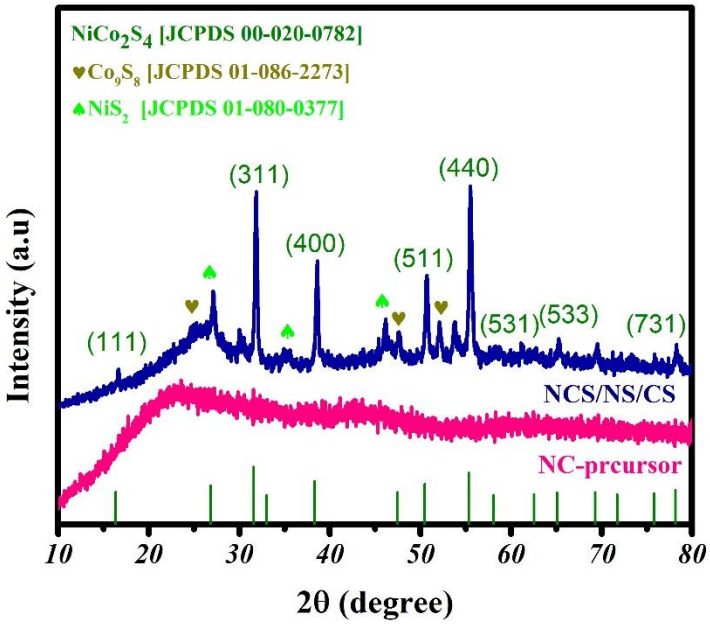

Fig. 2: **XRD patterns of NC-precursor and NCS/NS/CS.**

The morphology of the manufactured materials was examined using FE-SEM. As PEI is a carbon source during the synthesis process, Fig. 3a illustrates the carbon template insertion of the NC-precursor. The degradation of the PEI carbon template following the annealing of NC-precursor with S powder results in the appearance of NCS/NS/CS, which may improve the morphology of the NCS/NS/CS and produce the anticipated improved electrochemical performance, as demonstrated in Fig. 3b.

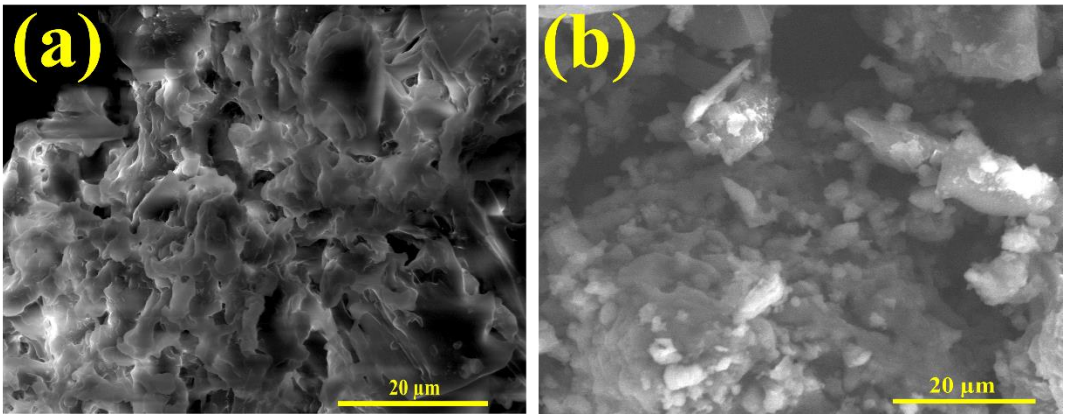

Fig. 3: FESEM micrograph of (a) NC-precursor and (b) NCS/NS/CS.

3.2. Electrochemical performance

A three-electrode set-up was used to examine the electrochemical behaviour of the manufactured electrodes. Fig. 4a reveals the CV curves within a -0.2 to 0.5 V potential range for the electrodes of NC-precursor and NCS/NS/CS at 50 mV s^{-1}. As contrasted to the NC-precursor electrode, the as-made NCS/NS/CS electrode appears to have a wider CV curve area and a higher current response, suggesting that NCS/NS/CS has a higher capacitance than the NC-precursor. The composite electrodes' findings show pair redox peaks, which point to the behaviour of a battery type [35]. This outcome is attributed to Faradic redox reactions being involved in the electrochemical storage process. The NCS/NS/CS electrode's CV curves are displayed in Fig. 4b at different scan rates (200–5) mVs^{-1} to show how the scan rate affects the electrochemical characteristics. Two peaks of redox are present in every CV curve, and when the scan rate rises, the symmetrical curve's shape reveals the battery type through its reversible charge-discharge behaviour. It is evident that when the scan rate rises, the redox current rises, and the peaks of oxidation and reduction move towards a high positive/negative potential, which

is due to the polarization of the electrode [36, 37]. We show that in the chemical reactions of NCS/NS/CS in KOH solution, the redox peaks (anodic and cathodic) that relate to redox reversible Faradaic reactions, including Ni^{2+}/Ni^{3+}, Co^{2+}/Co^{3+}, and Co^{3+}/Co^{4+} [20, 21, 38-41].

$$NiCo_2S_4 + OH^- + H_2O \leftrightarrow NiSOH + 2CoSOH + 2e^- \quad (6)$$

$$CoSOH + OH^- \leftrightarrow CoSO + H_2O + e^- \quad (7)$$

$$Co_9S_8 + OH^- \leftrightarrow Co_9S_8OH + e^- \quad (8)$$

$$Co_9S_8OH + OH^- \leftrightarrow Co_9S_8O + H_2O + e^- \quad (9)$$

$$NiS_2 + OH^- \leftrightarrow NiS_2OH + e^- \quad (10)$$

To elucidate how the scan rate influences the peak current, the Randles-Sevcik equation can be employed [42]. The linear correlation between peak current density (I) and the square root of the scan rate (v) reveals insight into the battery characteristics of the NCS/NS/CS as illustrated in Fig. 4c. The Dunn et al. equation can additionally be employed to ascertain if the process is diffusion-controlled or non-diffusion-limited by displaying the energy storage kinetics through the created electrodes from a CV profile [43, 44].

$$I(V) = k_1v + k_2v^{1/2} \quad (11)$$

Where I (V) stands for the current at a certain potential, v denotes the scan rate (mV s^{-1}), and k1 and k2 are the values associated with diffusion and non-diffusion current, respectively. It is possible to simplify the preceding equation to $i(V) = av^b$ [43]. The process is considered diffusion-controlled when b = 0.5 and surface capacitive when b = 1. From Fig. 4d, the values of b are 0.49 and 0.5, which correspond to the anodic and cathodic peaks of NCS/NS/CS. These readings, which are nearly 0.5, demonstrate the diffusion-controlled nature of the process and highlight the NCS/NS/CS electrode's battery-like behaviours. The good morphology and following extrinsic pseudocapacitance performance may be the cause of the divergence from 0.5.

By applying the technique of Trasattiet et al. [45-47], the total charge may be computed using the plot of 1/q vs. scan rate, as illustrated in Fig. 4e. At a low enough scan rate, since the ions require time to spread out and react, the NCS/NS/CS electrode displays an overall capacity of 250 C g^{-1}. The outer charge (q_{outer}), which is the charge stored (q) at a limitless scan rate, is

obtainable via the intercept of the capacity (q) vs. scan rate (v) plot. The outer (surface) charge of the NCS/NS/CS electrode is 26.5 C g^{-1}, as observed in Fig. 4f. As a result of this, 89.4% of diffusion-controlled Faradaic reactions by using the whole charge.

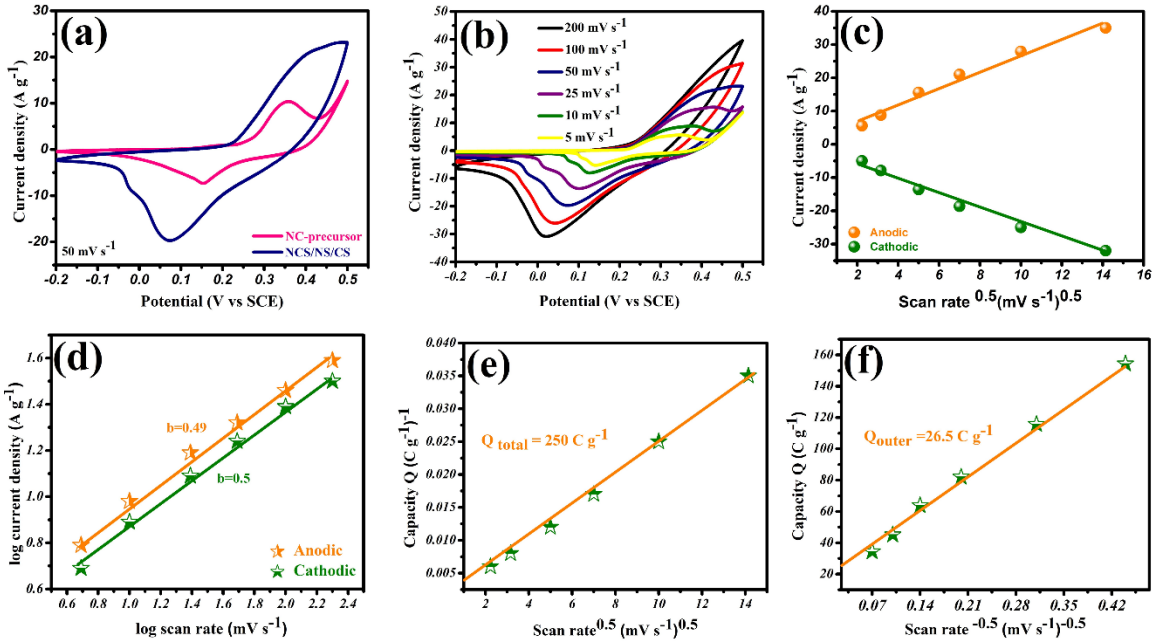

Fig. 4: (a) CV curves of NC-Precursor and NCS/NS/CS; (b) CV curves of NCS/NS/CS at different scan rates; (c) peak current density as a function of the square root of the scan rate; (d) dependence of log current on log scan rate; (e) plot of 1/q vs. scan rate$^{1/2}$ to find the total charge (q_{total}) stored by NCS/NS/CS; and (f) plot of q vs. scan rate$^{-1/2}$ to find the outer charge of NCS/NS/CS.

Fig. 5a illustrates the GCD curves for the NC-precursor and NCS/NS/CS electrodes at 1 A/g. The plateau-like potential profile of the GCD curves demonstrates that the supercapacitive performance is that of the Faradaic battery type. The curves show that NCS/NS/CS exhibits longer discharge times than NC-precursor, which suggests that their electrochemical features are superior. Additionally, for the NC-precursor, the values of capacitance and capacity are 63 F/g (26 C/g), and for the NCS/NS/CS, they are 301 F/g (123 C/g) at 1 A/g. These data show that the capacitance of the NCS/NS/CS electrode is higher than that of the NC-precursor electrode, recommending a notable development in electrochemical storage associated with enhanced morphology during annealing.

Fig. 5b reveals the NCS/NS/CS electrode's GCD curves at different current densities (0.5–10) A/g. The plateaus are noticeable and represent characteristics of a battery type. The two electrodes' Cs are displayed in Fig. 5c. The Cs and C values of the NCS/NS/CS are as follows: 326 F/g (135 C/g), 301 F/g (123 C/g), 271 F/g (109 C/g), 243 F/g (98 C/g), 222 F/g (92 C/g), 200 F/g (83 C/g), and 125 F/g (56 C/g), at 0.5, 1, 2, 3, 4, 5, and 10 A/g. As can be observed, when current density rises, capacity somewhat decreases. This behaviour can be explained by the distinct morphology of the created NCS/NS/CS electrode, even though the material is battery-type. This property makes extrinsic pseudocapacitance possible, which aids in maintaining the electrode's high capacity even when a large current density is applied [48].

EIS for NC-precursor and NCS/NS/CS is used at open circuit potential. Fig. 5d illustrates the fitting curve that was fitted using Zview^{TM} software. Every Nyquist plot has an equivalent series resistance (ESR). The ESR values for NC-precursor and NCS/NS/CS are 1.4 and 1.7 **Ω**, respectively. This indicates that the NC-precursor has a lower value than the NCS/NS/CS because the PEI-precursor has larger amounts of carbon and nitrogen. Also, it is noticed that the charge transfer resistance (Rct) for NCS/NS/CS is 5.4 **Ω** at high frequency, which is lower than that of the NC-precursor, which is 8 **Ω**. That suggests a fast rate of charge motion, which reflects an increase in capacitance following annealing. At low frequencies, the NC-precursor and NCS/NS/CS electrodes had Warburg resistance (W_R) values of 35 and 48, respectively. Because there are more active sites on the NCS/NS/CS electrode than on the NC-precursor electrode, the electrode's constant phase element (CPE_T) value is significantly greater [49, 50].

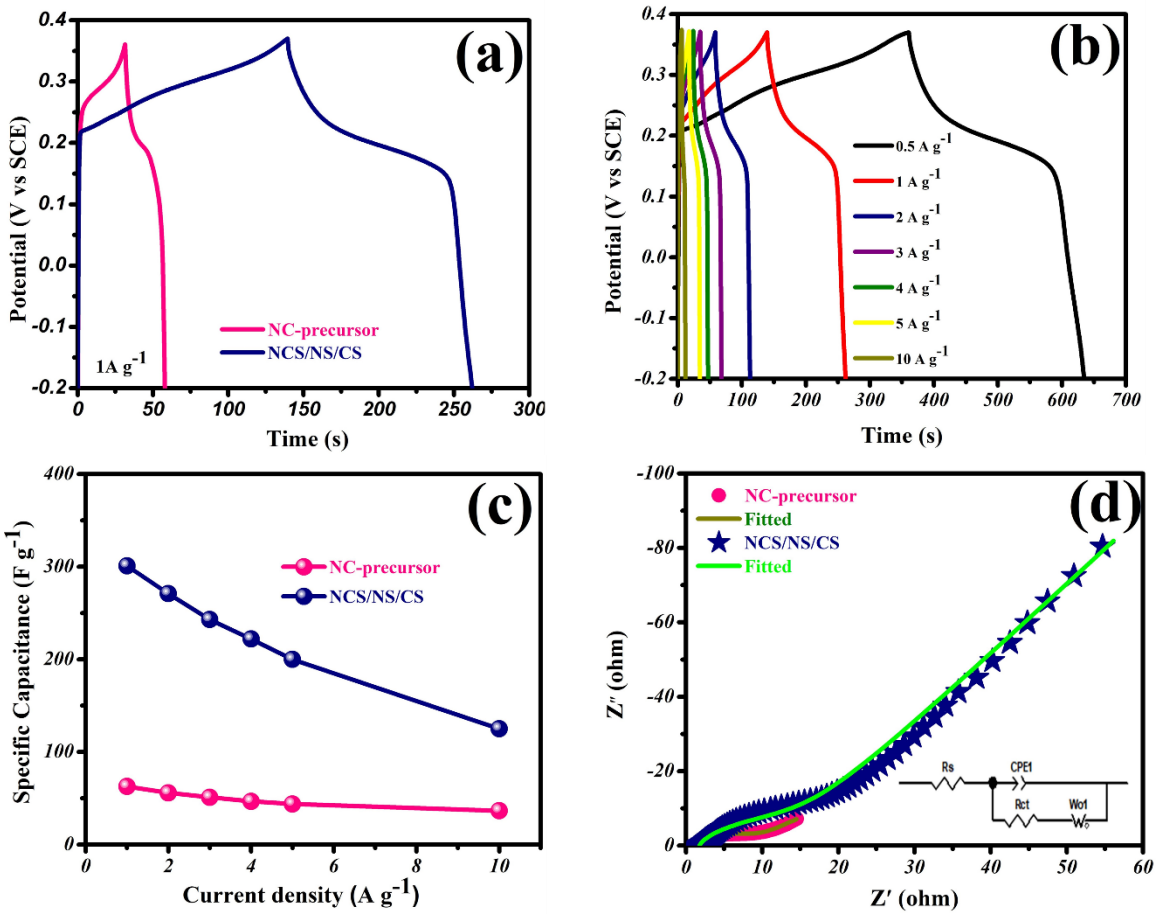

Fig. 5: (a) GCD of the NC-precursor and NCS/NS/CS; (b) GCD curves of the NCS/NS/CS at different current densities; (c) Specific capacitance of the NC-precursor and NCS/NS/CS; and (d) EIS plots of the NC-precursor and NCS/NS/CS.

Table (1): The EIS results of the NC-precursor and NCS/NS/CS. ([a] The capacitance when CPE_P = 1. [b] The constant phase element exponent. [c] The diffusion resistance (Warburg diffusion resistance). [d] The diffusion time constant; [e] A fractional exponent between 0 and 1).

Samples	Rs (Ω)	CPE_T [a]	CPE_P [b]	Rct (Ω)	W_R [c]	W_T [d]	W_P [e]
NC-precursor	1.4	0.00699	0.7566	8	35	20	0.5318
NCS/NS/CS	1.7	0.008	0.859	5.4	48	3.5	0.3555

For practical application in symmetric SCs. The NCS/NS/CS composite can be applied as the anode and cathode, with the formula NCS/NS/CS//NCS/NS/CS being established. The constructed symmetric device's CV curves are shown in Fig. 6a, with variant scan speeds ranging from 200–10 mV s^{-1} within a constant voltage window (0-1.5 V). The significant redox reaction noticed suggests that the constructed symmetric device has Faradaic charge storage performance. Moreover, the built device's GCD behaviour is shown in Fig. 6b at applied current densities of 1 to 5 A/g. The device exhibits nonlinear plateaus that point to its battery-type Faradaic feature. From discharge curves, the specific capacity of the device may be estimated; with a current density of 1, 2, 3, 4, and 5 A/g, respectively, the computed values are 114.8, 64.8, 43.7, 30, and 22 C g^{-1}. The device's EIS test is shown in Fig. 6c, where the ESR value is 12.5 and shows a good value of Rct. Additionally, a lower vertical line demonstrates good electrolyte ion transport, as shown in the Ragon plot for a symmetric device in Fig. 6d, reaching the superior energy density of 18.9 Wh k/g at a power density of 592 W k/g.

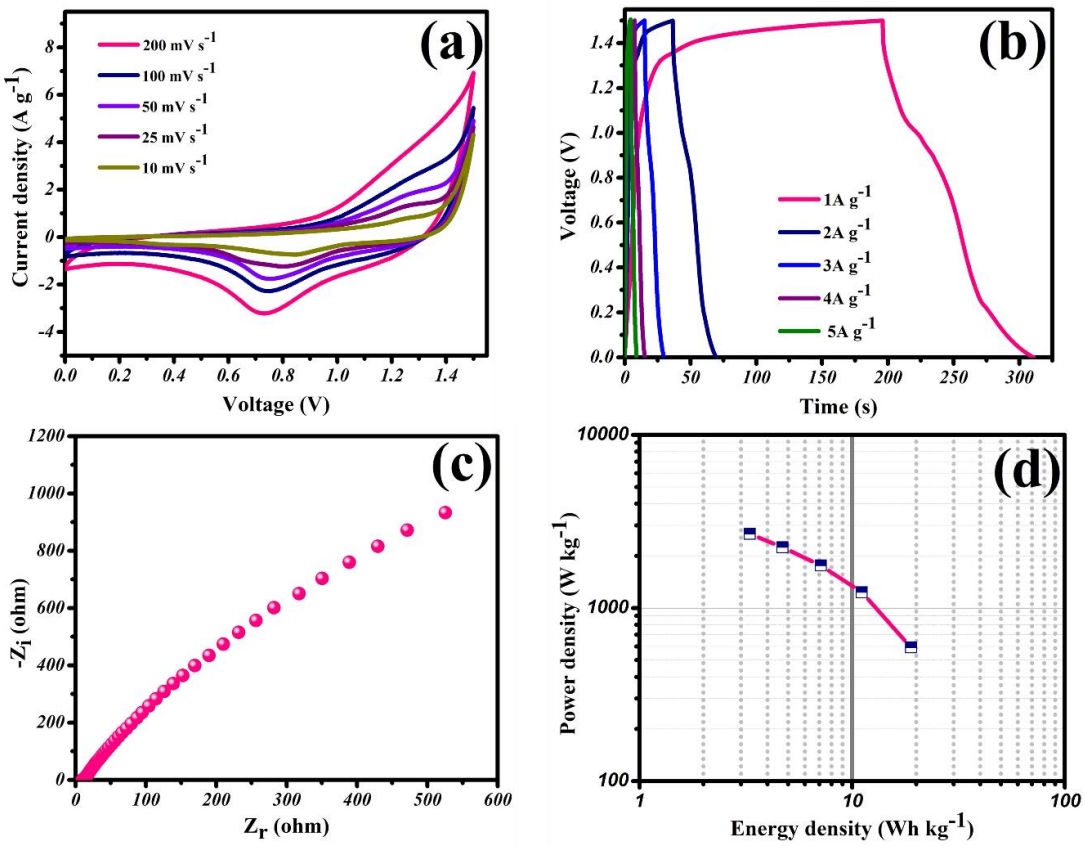

Fig. 6: (a) CV curves of NCS/NS/CS//NCS/NS/CS; (b) GCD curves of NCS/NS/CS//NCS/NS/CS; (c) EIS spectrum; and (d) Ragone plot for the symmetric device.

4. Conclusions

In this study, we manufactured a $NiCo_2S_4/NiS_2/Co_9S_8$ nanocomposite (NCS/NS/CS) via using polyethyleneimine as a source of carbon and nitrogen and worked as a template by solvothermal technique to synthesise NC-precursor. After that, we annealed the NC-precursor with S powder for two hours at 300 °C in an argon atmosphere. The enhanced morphology, as shown from FESEM, and NCS/NS/CS electrode conductivity allow for fast ion transport, giving them an excellent electrochemical energy storage feature. The NCS/NS/CS nanocomposite displays a capacitance of 326 F/g at 0.5 A/g. Additionally, utilizing NCS/NS/CS electrodes for each of the positive and negative electrodes, an NCS/NS/CS//NCS/NS/CS symmetric device was created, providing an exceptional 18.9 Wh k/g of specific energy at a specific power of 529 W k/g at 1 A/g.

5. Declaration of competing interest

The authors declare that they have no known competing financial interests or personal relationships that could have appeared to influence the work reported in this paper.

6. Acknowledgments

The authors are immensely thankful to the Chemistry Department in the Faculty of Women for Arts, Science, Education, Ain Shams University, and Tabbin Institute for Metallurgical Studies for providing facilities to carry out the work.

References

[1] Siwatch, P., K. Sharma, and S. Tripathi, Facile synthesis of NiCo2O4 quantum dots for asymmetric supercapacitor. Electrochimica Acta, 2020. 329: p. 135084.

[2] Poonam, et al., Review of supercapacitors: Materials and devices. Journal of Energy Storage, 2019. 21: p. 801-825.

[3] Ma, Z., et al., Nitrogen and sulfur co-doped porous carbon derived from bio-waste as a promising electrocatalyst for zinc-air battery. Energy, 2018. 143: p. 43-55.

[4] Pal, M., et al., Ultra high supercapacitance of ultra small Co3O4 nanocubes. Energy, 2016. 103: p. 481-486.

[5] He, P., et al., Controllable synthesis of Ni–Co–Mn multi-component metal oxides with various morphologies for high-performance flexible supercapacitors. RSC Advances, 2017. 7(39): p. 24353-24358.

[6] Xiang, C., et al., Simple synthesis of graphene-doped flower-like cobalt–nickel–tungsten–boron oxides with self-oxidation for high-performance supercapacitors. Journal of Materials Chemistry A, 2017. 5(20): p. 9907-9916.

[7] González, A., et al., Review on supercapacitors: Technologies and materials. Renewable and Sustainable Energy Reviews, 2016. 58: p. 1189-1206.

[8] Liu, S., et al., Controllable sulfuration engineered NiO nanosheets with enhanced capacitance for high rate supercapacitors. Journal of Materials Chemistry A, 2017. 5(9): p. 4543-4549.

[9] Liu, Y., K. Shi, and I. Zhitomirsky, Asymmetric supercapacitor, based on composite MnO2-graphene and N-doped activated carbon coated carbon nanotube electrodes. Electrochimica Acta, 2017. 233: p. 142-150.

[10] He, X., et al., Hierarchical NiCo2O4@NiCoAl-layered double hydroxide core/shell nanoforest arrays as advanced electrodes for high-performance asymmetric supercapacitors. Journal of Alloys and Compounds, 2017. 724: p. 130-138.

[11] Abdel-Salam, A.I., et al., Designing a hierarchical structure of nickel-cobalt-sulfide decorated on electrospun N-doped carbon nanofiber as an efficient electrode material for hybrid supercapacitors. International Journal of Hydrogen Energy, 2023. 48(14): p. 5463-5477.

[12] Noori, A., et al., Towards establishing standard performance metrics for batteries, supercapacitors and beyond. Chemical Society Reviews, 2019. 48(5): p. 1272-1341.

[13] Attia, S.Y., et al., Supercapacitor electrode materials: addressing challenges in mechanism and charge storage. Reviews in Inorganic Chemistry, 2022. 42(1): p. 53-88.

[14] Mariappan, C.R., et al., Synthesis and electrochemical properties of rGO/polypyrrole/ferrites nanocomposites obtained via a hydrothermal route for hybrid aqueous supercapacitors. Journal of Electroanalytical Chemistry, 2019. 845: p. 72-83.

[15] Zhai, R., et al., Construction of NiCo2S4 heterostructure based on electrochemically exfoliated graphene for high-performance hybrid supercapacitor electrode. Journal of Alloys and Compounds, 2020. 845: p. 156164.

[16] Yu, X.-Y., L. Yu, and X.W. Lou, Metal Sulfide Hollow Nanostructures for Electrochemical Energy Storage. Advanced Energy Materials, 2016. 6(3): p. 1501333.

[17] Hou, L., et al., Hollow mesoporous hetero-NiCo2S4/Co9S8 submicro-spindles: unusual formation and excellent pseudocapacitance towards hybrid supercapacitors. Journal of Materials Chemistry A, 2017. 5(1): p. 133-144.

[18] Huang, X., et al., Formation of hierarchical core-shell hollow Co3S4@NiCo2S4 nanocages with enhanced performance for supercapacitor. Journal of Alloys and Compounds, 2023. 947: p. 169413.

[19] Liu, Y., et al., MOF-derived Co9S8 polyhedrons on NiCo2S4 nanowires for high-performance hybrid supercapacitors. Inorganic Chemistry Frontiers, 2020. 7(21): p. 4092-4100.

[20] Xu, R., et al., Two-step hydrothermal synthesis of NiCo2S4/Co9S8 nanorods on nickel foam for high energy density asymmetric supercapacitors. Applied Surface Science, 2018. 434: p. 861-870.

[21] Han, X., et al., Template synthesis of NiCo2S4/Co9S8 hollow spheres for high-performance asymmetric supercapacitors. Chemical Engineering Journal, 2019. 368: p. 513-524.

[22] Sui, Y., et al., High Energy Density Asymmetric Supercapacitor Based ZnS/NiCo2S4/Co9S8 Nanotube Composites Materials. Advanced Materials Interfaces, 2018. 5(12): p. 1800018.

[23] Zhao, J., et al., Sulfur-deficient Co9S8/Ni3S2 nanoflakes anchored on N-doped graphene nanotubes as high-performance electrode materials for asymmetric supercapacitors. Science China Technological Sciences, 2020. 63(4): p. 675-685.

[24] Zhang, X., et al., Design of thin-layer porous nickel cobalt sulfide for high-performance asymmetric supercapacitors. Journal of Alloys and Compounds, 2023. 945: p. 168902.

[25] Wang, F., et al., One-step hydrothermal synthesis of sandwich-type NiCo2S4@ reduced graphene oxide composite as active electrode material for supercapacitors. Applied Surface Science, 2017. 425: p. 180-187.

[26] Xiong, X., et al., Controlled synthesis of NiCo2S4 nanostructured arrays on carbon fiber paper for high-performance pseudocapacitors. Nano Energy, 2015. 16: p. 71-80.

[27] Govindasamy, M., et al., Fabrication of hierarchical NiCo2S4@ CoS2 nanostructures on highly conductive flexible carbon cloth substrate as a hybrid electrode material for supercapacitors with enhanced electrochemical performance. Electrochimica Acta, 2019. 293: p. 328-337.

[28] Zhang, J., et al., Modified polyethyleneimine with abundant N/O/S-heteroatoms and aromatic segments: Convenient synthesis via sulfur-isocyanide-amine multicomponent reaction and application in high-performance iodine capture. European Polymer Journal, 2024. 205: p. 112724.

[29] Chen, Z., et al., Recent advancements in polyethyleneimine-based materials and their biomedical, biotechnology, and biomaterial applications. J Mater Chem B, 2020. 8(15): p. 2951-2973.

[30] Diab, M.A., et al., Design of multifunctional 1D/2D polypyrrole nanotubes@pg-C3N4 binary nanocomposite for removal of mercury (Hg2+) from wastewater and supercapacitor applications. Journal of Industrial and Engineering Chemistry, 2023.

[31] El-Sabban, H.A., et al., Rational design of MoS2 nanoflowers grafted highly porous functionalized woody pulp-derived biochar for sustainable energy storage devices. Fuel, 2024. 359: p. 130485.

[32] Attia, S.Y., et al., A single-step synthesis and direct growth of microspheres containing the nanoflakes-like structure of Zn0. 76Co0. 24S as a high-performance electrode for supercapacitors. Journal of Energy Storage, 2020. 29: p. 101349.

[33] Shao, Y., et al., Design and mechanisms of asymmetric supercapacitors. Chemical reviews, 2018. 118(18): p. 9233-9280.

[34] Mostafa, R.E., et al., Novel fabrication of a nanostructured NiCo2S4/Ni/Ni9S8 composite for energy storage applications. The Bulletin Tabbin Institute for Metallurgical Studies (TIMS), 2023.

[35] Wang, H., et al., Rational design of porous NiCo2S4 nanotubes for hybrid supercapacitor. Current Applied Physics, 2022. 35: p. 7-15.

[36] Abdel-Salam, A.I., et al., Facile one-step hydrothermal method for NiCo2S4/rGO nanocomposite synthesis for efficient hybrid supercapacitor electrodes. Materials Chemistry and Physics, 2022. 277: p. 125554.

[37] Ahmed, S.Y., et al., High electrochemical energy-storage performance promoted by SnSe nanorods anchored on rGO nanosheets. Journal of Electroanalytical Chemistry, 2021. 883: p. 115063.

[38] Li, L., et al., Carbon@ NiCo 2 S 4 nanorods: an excellent electrode material for supercapacitors. RSC advances, 2015. 5(101): p. 83408-83414.

[39] Meng, Y., et al., Uniform P doped Co–Ni–S nanostructures for asymmetric supercapacitors with ultra-high energy densities. Nanoscale, 2019. 11(2): p. 688-697.

[40] Wang, Y., et al., Rational design of multi-shelled CoO/Co9S8 hollow microspheres for high-performance hybrid supercapacitors. Journal of Materials Chemistry A, 2017. 5(35): p. 18448-18456.

[41] Xiao, J., et al., Heterostructure NiS2/NiCo2S4 nanosheets array on carbon nanotubes sponge electrode with high specific capacitance for supercapacitors. Journal of Power Sources, 2022. 518: p. 230763.

[42] Frackowiak, E. and F. Béguin, Carbon materials for the electrochemical storage of energy in capacitors. Carbon, 2001. 39(6): p. 937-950.

[43] Wang, J., et al., Pseudocapacitive Contributions to Electrochemical Energy Storage in TiO2 (Anatase) Nanoparticles. The Journal of Physical Chemistry C, 2007. 111(40): p. 14925-14931.

[44] Abuelftooh, A.M., et al., High specific energy supercapacitor electrode prepared from MnS/Ni 3 S 2 composite grown on nickel foam. New Journal of Chemistry, 2021. 45(39): p. 18641-18650.

[45] Abuelftooh, A., et al., A three-dimensional directly grown hierarchical graces-like Nickel Manganese Selenide for high-performance Li-ion battery and supercapacitor electrodes. Materials Today Chemistry, 2022. 26: p. 101187.

[46] Singh, A.K., et al., High-Performance Supercapacitor Electrode Based on Cobalt Oxide–Manganese Dioxide–Nickel Oxide Ternary 1D Hybrid Nanotubes. ACS Applied Materials & Interfaces, 2016. 8(32): p. 20786-20792.

[47] Sankar, K.V. and R.K. Selvan, The ternary MnFe2O4/graphene/polyaniline hybrid composite as negative electrode for supercapacitors. Journal of Power Sources, 2015. 275: p. 399-407.

[48] Abuelftooh, A.M., et al., High specific energy supercapacitor electrode prepared from MnS/Ni3S2 composite grown on nickel foam. New Journal of Chemistry, 2021. 45(39): p. 18641-18650.

[49] Eldoma, M.A., et al., Enhancing photocatalytic performance of Co-TiO2 and Mo-TiO2-based catalysts through defect engineering and doping: A study on the degradation of organic pollutants under UV light. Journal of Photochemistry and Photobiology A: Chemistry, 2024. 446: p. 115164.

[50] Bredar, A.R.C., et al., Electrochemical Impedance Spectroscopy of Metal Oxide Electrodes for Energy Applications. ACS Applied Energy Materials, 2020. 3(1): p. 66-98.

المخلص العربي

تجميع مركب $NiCo_2S_4/NiS_2/Co_9S_8$ ذو البنية النانوية لتحسين الأداء الكهروكيميائي في المكثفات الفائقة المتماثلة.

ريهام ايهاب مصطفي[١,*], سهير سعد محمود [١], نورا سعد طنطاوي [١], سعد جمعه محمد [٢]

[١]قسم الكيمياء – كلية البنات للعلوم والأداب والتربية – جامعة عين شمس – الفاهره – مصر
[٢] قسم التعدين والهندسه - معهد التبين للدراسات المعدنية – حلوان – القاهره - مصر

الملخص العربي:

باعتبارها مواد قطب كهربائي لأجهزة تخزين الطاقة فائقة السعة، فإن كبريتيدات الفلزات الانتقالية ثنائية المعدن (TMSs) تظهر إمكانات كبيرة. ومع ذلك، لمواصلة تعزيز الأداء الكهروكيميائي، لا تزال هناك حاجة إلى تطوير تقنيات اصطناعية فعالة لهندسة قطب كهربائي مفيدة. في هذه الدراسة، استخدمنا البولي إيثيلين أمين بتقنية المذيبات الحرارية لتخليق مركب نانوي $NiCo_2S_4/NiSe_2/Co_9S_8$ (NCS/NS/CS). بعد ذلك، قمنا بعملية تلدين لـ NC-precursorمع مصدر كبريتيد عند ٣٠٠ درجة مئوية لمدة ساعتين في وجود غاز الأرجون. تسمح الموصلية العالية ومساحة السطح المحسنة للقطب الكهربائي NCS/NS/CS بنقل الأيونات بسرعة، مما يمنحها ميزة ممتازة لتخزين الطاقة الكهروكيميائية. عند كثافة تيار تبلغ ٠,٥ امبير/جرام، يُظهر المركب النانوي NCS/NS/CS سعة محددة عالية تبلغ ٣٢٦ فاراد/جرام. بالإضافة إلى ذلك، باستخدام أقطاب NCS/CS/NS لكل من الأقطاب الكهربائية الموجبة والسالبة، تم إنشاء جهاز متماثل NCS/NS/CS//NCS/NS/CS، مما يوفر طاقة استثنائية تبلغ ١٨,٩ وات.ساعة/كجم من طاقة محددة بقدرة محددة ٥٢٩ وات/ كجم بكثافة تيار حالية تبلغ ١امبير/جرام.